Mem. S.A.It. Vol. 95, 48

Memorie della

RIIFS, Study of a Rugged Imaging Fourier Spectrometer for planetary applications

G. Bellucci[1], M. De Luca[2], B. Saggin[3,5], A. Appiani[3], S. Iarossi[2], F. Oliva[1], E. D'Aversa[1], M. Giuranna[1], F.G. Carrozzo[1], F. Altieri[1], F. Lo Castro[2], L. Bucciantini[4], C. Mastrandrea[4]

[1] INAF – Istituto di Astrofisica e Planetologia Spaziali, Via del Fosso del Cavaliere 100, 00133, Rome - Italy e-mail: giancarlo.bellucci@inaf.it
[2] CNR – Istituto di Ingegneria del Mare, Via del Fosso del Cavaliere 100, 00133, Rome - Italy
[3] Department of Mechanical Engineering, Politecnico di Milano, Polo Territoriale di Lecco, Via Gaetano Previati, 1/c, 23900 Lecco - Italy
[4] Leonardo Finmeccanica, Via Delle Officine Galileo, 1, 50013 Campi Bisenzio Firenze - Italy
[5] Dipartimento di Ingegneria Industriale, Università degli Studi di Padova, CISAS "G. Colombo", via Venezia 1, 35131 Padova - Italy

Received: 26 March 2024; Accepted: 27 May 2024

Abstract. Aim of the study has been to implement innovative technical solutions which will allow generating a new class of compact Fourier Transform spectrometers (FTS), both for in situ and orbiter operations. In particular, we wanted to generate an instrument configuration flexible enough to be adapted, with minor modifications, to several planetary scenarios and targets. During the study, we have identified the main constrains in the design and which subsystems must be modified and/or adapted to better investigate the selected planetary target. Functioning in harsh mechanical and thermal environment is nowadays incompatible with FTS commonly associated to vibration free and thermally stable environments, even for ground applications. The implementation of time-based sampling techniques associated to newly developed data processing algorithms and the application of phase-based calibration procedures promise to strongly relax the FTS environmental requirements.

Key words. Planets: Satellites: Minor bodies: Spectroscopy, Surfaces and Atmospheres

1. Introduction

Studies of the mineral chemistry of planets, moons or asteroids are essential to understand the history of their crusts, but also to grasp a more global view of the history of our Solar System. Similarly, monitoring the composition of the atmospheres of such bodies, provides a wealth of information on the processes occurring today but also on the history of the atmospheres, and the relation existing between the volatiles trapped within the surface and those present in the atmospheric reser-

voirs. Infrared spectroscopy is a useful remote-sensing tool for the detection and characterization of surfaces and for the monitoring of the atmospheres. Several types of instruments have been developed and have already flown on planetary missions (e.g. Hanel et al. (2003). Although all are based on the use of spectroscopy, they have all been developed around different designs with different scientific objectives (e.g. Multi-spectral filter/grating spectrometers, Echelle spectrometers, FTS, etc). The aim of the study described here was to implement innovative technical solutions which will allow generating a new class of compact FTS instruments, for both in situ and orbiter operations. The study was conducted under an Italian Space Agency (ASI) contract (Attività di Studio per la comunità scientifica nazionale Sole, Sistema solare e Esopianeti, ASI-INAF n.2018-16-HH.0). Functioning in harsh mechanical and thermal environment is nowadays incompatible with FTS commonly associated to vibration free and thermally stable environments, even for ground applications. The implementation of time-based sampling techniques associated to newly developed data processing algorithms and the application of phase-based calibration procedures, promise to strongly relax the FTS environmental requirements. Moreover, the new configuration will allow building the FTS as an optical head, the interferometer, including as electronics just the detectors preamplifiers, run by a Digital Processing Unit (DPU) with Data Acquisition (DAQ) capability e.g. the main electronic of a rover, without a dedicated electronic unit. This implementation would make it compatible with the thermal and radiation environments typical of planetary surfaces conditions and critical to electronic units survival. An additional study goal was to widen the instrument scientific performances by including imaging capabilities; this will entail the design of a telescope to be coupled with the interferometer to meet the angular resolution requirements. Most of the activities have been developed at INAF-IAPS, CNR-INM and Politecnico di Milano, with a contribution by Italian Industry on the telescope architecture definition and space qualification aspects.

2. Requirements

In general, the science objectives that can be afforded with a FTS can be grouped in two basic categories:

- Retrievals of vertical profiles of atmospheric properties, like temperature, pressure, gases and aerosols composition and abundance, including the Earth's environmental monitoring of greenhouse gases and pollutants;

- Studies of solid/liquid surfaces composition and micro-physical properties, as well as the related geological processes.

These studies can be conducted from both orbiter, rover surface platforms and balloons. Atmospheric sounding makes use of the principles of radiative transfer through an absorbing-transmitting medium, and mathematical inversion methods are used to determine the profile of temperature and gases' abundance versus altitude which led to the observed radiation. The instrument's task is to measure the received radiation with the instrumental accuracy and spectral resolution dictated by the spectroscopic properties of the medium and the desired profile, since gases absorption lines are always spectrally narrow. Note that the spectral resolution impacts the vertical resolution of the profile.

Depending on the observing wavelength, the measured radiation can be either the Sun-reflected or thermally emitted by the surface-atmosphere system. Surface studies, allowed in spectral ranges not totally absorbed by the atmosphere, are performed by comparing the measured spectra with mineralogical libraries and radiative transfer models. Such an approach has proven quite useful in remote examination of planetary surfaces and atmospheres for solid materials, water ice, dust clouds, SO_2 ice crystals, etc. We start the study with an already defined spectral range. We divide this wide range in SWIR (2–5 μm) and LWIR (5–25 μm). This because most of the absorption features of gases and rocks fall in this range and the thermal emission of several planetary bodies peaks in this range. In the SWIR, a

minimum single-measurement signal-to-noise ratio (SNR) of 30 should allow a wide mapping of the stronger spectral features for both planetary surfaces and main atmospheric gases. As far as spectral resolution is concerned, the SWIR spectral resolving power must be adequate to resolve narrow gases absorption features. For example, a resolving power of 1000 at 2 μm and 200 at 10 μm will allow to resolve the narrow absorption lines of the most common gases, like CO_2, H_2O and O_3. As far as the LWIR domain is concerned, the compositional requirement for a FTS investigation is to determine mineral abundances in mixtures to $\pm 10\%$ accuracy. Moreover, the emissivities of moderate absorption bands of medium-grained particulates ($\sim$ 100 μm) need a precision of about 5%. Extensive experience with lab and spacecraft data has shown that, in order to identify components, FTS requires a radiometric precision of 1/16 of the band depth (or a science to noise ratio of 16, e.g. (Ramsey & Christensen (1998)); (Hamilton & Christensen (2000)); (Christensen et al. (2001)); (Rogers et al. (2007)). This requirement produces an emissivity precision requirement, stated as the Noise Equivalent Delta Emissivity (NEDϵ), equal to 0.05×1/16=0.003125. The NEDϵ is equal to the inverse of the signal-to-noise ratio (SNR), giving a minimum requirement of SNR=320. Laboratory and spacecraft experience have also shown that the absolute emissivity requirement is $\sim$ 10% of the emissivity, primarily to minimize spectral slopes, giving an absolute emissivity requirement of 0.9×0.1=0.09. Naturally, science requirements depend on specific science objectives. Here we want to identify a baseline configuration within some mass and volume constraints, which can be adapted with minor modification to specific scientific scenarios.

2.1. Summary of science requirements

On the basis of the above-mentioned discussion, the instrument should have the following scientific basic requirements:

- Spectral coverage: 2–25 μm;
- A resolving power of at least 1000 in the SWIR spectral range;
- A resolving power of at least 20-100 in the LWIR spectral range;
- Field of view (FOV): $\leq 1°$;
- Signal to noise: $\geq$ 30 in the SWIR and $\geq$ 300 in the LWIR spectral range

The instrument should be compact and modular to be easily adapted to different mission scenarios. Based on the various planetary targets (Moon, Mars, asteroids, etc.), the expected spectral range and signal to noise ratio will be different. For this reason, while maintaining the same optical design, it is envisaged to use different detectors to meet the SNR requirements. Moreover, the thermo-mechanical design should foresee the possibility of cooling the instrument to decrease the effect of instrument thermal background. We have then individuated two basic instrument architectures, the spectral coverage being defined by both detector sensitivity and optics transmission. The configuration characteristics are the following:

- Total dimensions = $10 \times 10 \times 20$ cm;
- Useful spectral range of the spectrometer = 2 - 25 μm;
- Resolving power = 1000 at 2 μm and 200 at 10 μm ;
- Measurement time = 3 seconds;
- Configuration # 1 (SWIR) = matrix consisting of 10×10 pixels of 100 μm, covering the range 2 - 5 μm; the sensor can be either cooled or at room temperature; available detector technologies are PbS, PbSe, InGaAS, HgCdTe.
- Configuration # 2 (LWIR) = matrix consisting of 10×10 pixels of 100 μm, covering the range 5 - 25 μm; the sensor can be either cooled or at room temperature; available detector technologies are microbolometer, pyroelectric, thermopile and HgCdTe. The spectral range of this configuration can be

extended above 25 μm by using a proper detector (e.g. pyroelectric or thermopile) and optics transparent at the required wavelengths.

- Telescope aperture = 8 cm;
- F-number = 2;
- Opening of the cubic mirrors = 2.54 cm;
- Field of view (FOV) = 0.5°;
- Instantaneous field of view (IFOV) = 0.05°;
- Total optical efficiency (telescope + interferometer): > 15% (sensor efficiencies are excluded);
- Optical quality ≤ 150 μm over the entire useful field (maximum spot size on the focal plane).
- Mass budget ≤ 5 kg

In Figure 1 we show the sensor detectivity (expressed by using the figure of merit D*, Henini & Razeghi (2002)) necessary to reach the minimum SNR in each wavelength range. The black curves indicate the spectrometer temperature needed to minimize the thermal background, allowing to reach the minimum SNR. The wavelength where both colored and black curves cross each other, provide the required spectrometer temperature. For inner planets and Mars, the instrument can be at room temperature and detectivities are reachable with detectors working either at room temperature or few tens degree below 0 °C (e.g. Henini & Razeghi (2002)). Dark asteroids and in general farthest and coldest object require both instrument cooling ad more sensitive detectors.

Figure 2 shows the instrument configuration and its optical performances on the overall field of view. The instrument is composed by a three mirror anastigmat (TMA) telescope coupled to a double pendulum interferometer. A laser diode at 635 nm is present to correctly sample the interferogram. The interferometer is inherited from the MIMA design (Bellucci et al. (2007)) which has been qualified from + 50 °C down to -130 °C. On Figure 2 (right) the optical spot diagrams are shown, indicating that the imaging performances are met on the assumed detector matrix. In the following we report some technical details about both the mechanical and electronics aspects.

3. Structural design

The RIIFS instrument is composed by two main parts: the telescope and the interferometer. The telescope is a newly developed component therefore the main activity has been the development of a basic structure configuration to define the mass budget and identify the overall volume envelope. The interferometer conversely inherits the development of the MIMA instrument Bellucci et al. (2007), Saggin et al. (2007a), Fonti et al. (2007), a spectrometer designed to map the mineralogical composition of the Martian surface and analyze its atmosphere, whose project was based on the use of light alloys with high mechanical properties machined mainly through chip removal and Electrical Discharge Machining (EDM). In this work the main mechanical components of the instrument have been redesigned considering the adoption Additive Manufacturing (AM) technology for the production. AM is a new technique now under development and assessment for space applications, not available at the time of the original design. The goal of the new development is obtaining structures with comparable or possibly improved mechanical performances but lower mass, exploiting tools such as Topology Optimization (TO), which provides efficient geometries but often not manufacturable with conventional techniques. The MIMA structure was optimized in the 2008 phase A/B development. The structure is already quite light in comparison to similar instruments, so the actual margins of improvements are seen in the change of manufacturing technology: from aluminum alloy milled structure to the metal AM technology using aluminum alloys. The structural design has been performed under the following requirements derived from MIMA design:

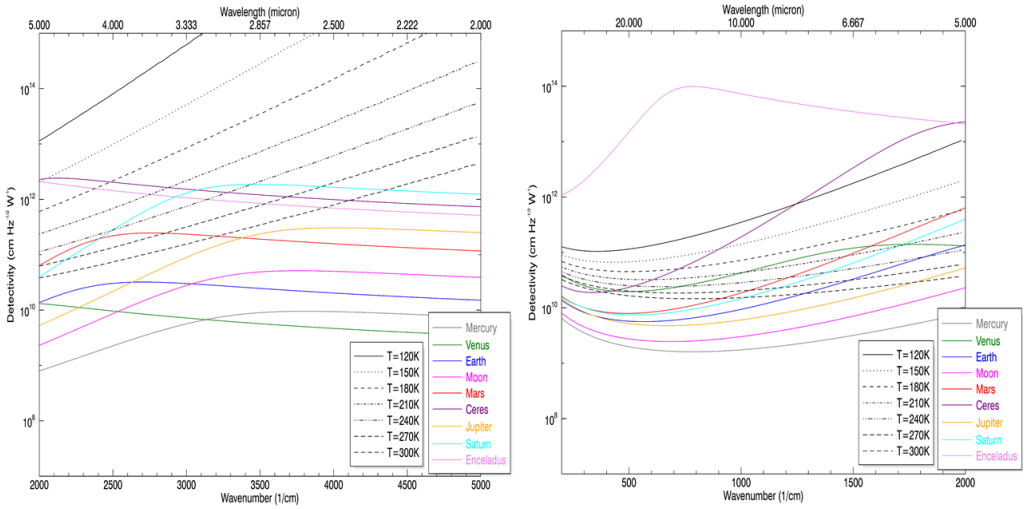

Fig. 1. Figures show the sensor detectivities (D*) necessary to reach a minimum SNR=30 for instrument configuration #1 (left) and SNR=300 for instrument configuration #2 (right). The black lines indicate the instrument temperature necessary to meet the minimum SNR (either 30 or 300). The wavelength where both colored and black curves cross each other, provide the required spectrometer temperature. Typical brightness temperature values and albedo/emissivities are assumed for the considered planetary bodies.

– First natural frequency higher than 150 Hz to avoid coupling with the sine excitation generated by the launcher lower resonances;

– Mechanical resistance against a dynamic load corresponding to hundred times the Earth's gravitational acceleration (g) acting along every direction.

The assessment of the mechanical resistance are often presented in terms of Margin of Safety (MoS), an index defined as:

$$MoS = \frac{\sigma_y}{(FoS \times \sigma_{VM})} - 1$$

where σ_y is the yield strength of the material, σ_{VM} is the maximum observed Von Mises stress and FoS is a safety factor. Positive value of MoS indicates that the component can withstand the applied load. In the following, at first the design of new components which were not present in the original instrument will be presented. The assembly is composed by the instrument base and box envelope, containing the Three Mirror Anastigmat (TMA) telescope and the interferometer. Then, the redesign of interferometer components directly derived from the original design will be discussed, i.e., the cubic mirror holdings and Optical Bench (OB).

3.1. MIMA design

The optics dimensions and disposition has been defined in the optical study provided as input for the thermo-mechanical design. All the elements (TMA mirrors and MIMA spectrometer) have been connected to a plate made with Al7075-T6 material and could be fitted in a box having dimensions of 270 mm x 178 mm x 137 mm. External walls 0.5 mm thick have been added, leaving a window for the optical beam entering the telescope. In this study the structures are modeled as equivalent plates with the goal of assessing the mass and volume

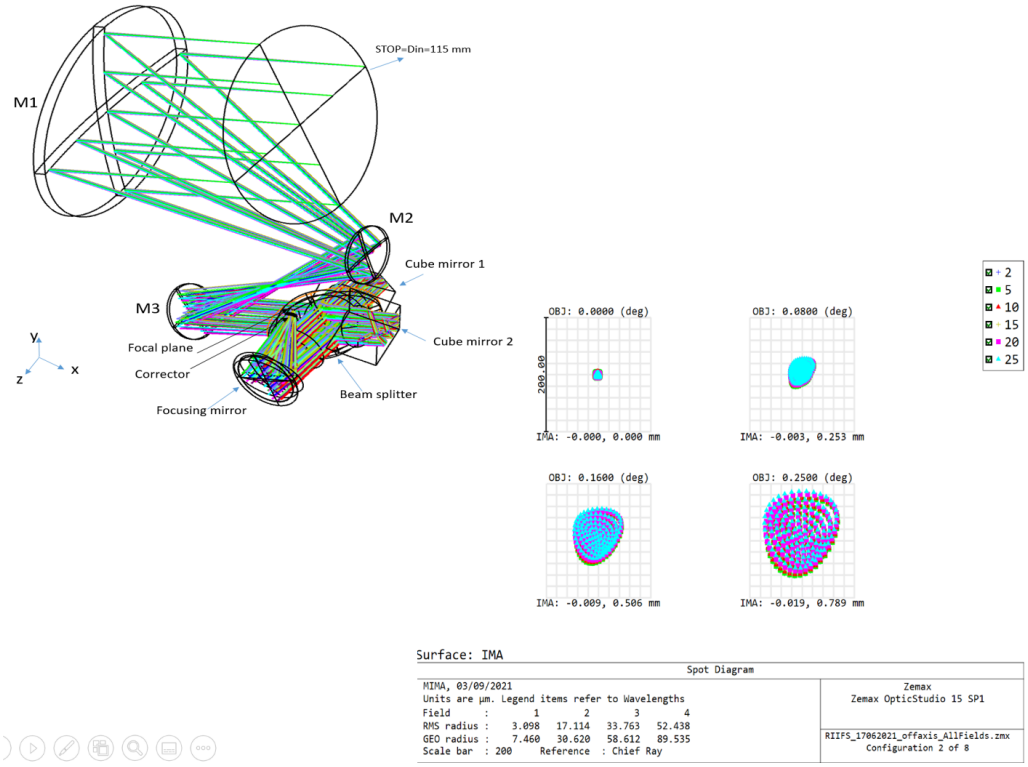

Fig. 2. Left) Optical layout of the instrument. The main parts are the TMA telescope and the double pendulum interferometer. Right) Spot diagrams on the detector for the entire spectral range (2 – 25 μm).

constraints. The following Figure 3 shows the instrument assembly without and with the box.

As first structure evolution stiffening ribs have been added to the plates on the top and external walls of the structure, while some material has been removed from the base plate leaving diagonal ribs. A parametric analysis has been conducted by means of FE analyses on the ribs dimensions to find values for these geometrical elements which were satisfactory from a dynamic behavior point of view. Following this activity, static analyses have been conducted on the selected geometry considering the quasi-static loading. Following Figure 4 and Table 1 summarize the results, which are compliant with the design requirements.

3.2. TMA components design and optimization

Both mirrors' structures and their supports have undergone design and optimization. The diameters of the optics, defined by the optical design of the instrument, were fixed to 127 mm, 34 mm and 32 mm for the sub-assemblies defined to as Mirror 1, Mirror 2 and Mirror 3 respectively. The thickness-to-diameter ratio was assumed 1:10 for all of them. Two types of compliant mountings were adopted, given the difference in size of the mirrors. For the smallest mirrors, i.e., Mirror 2 and 3, three equally spaced integral flexures embedded in a mounting ring were adopted, while for Mirror 1 the adopted design was based on back flexures. In particular, for Mirror 3 the adopted design allowed to obtain a mass reduction of about 47%

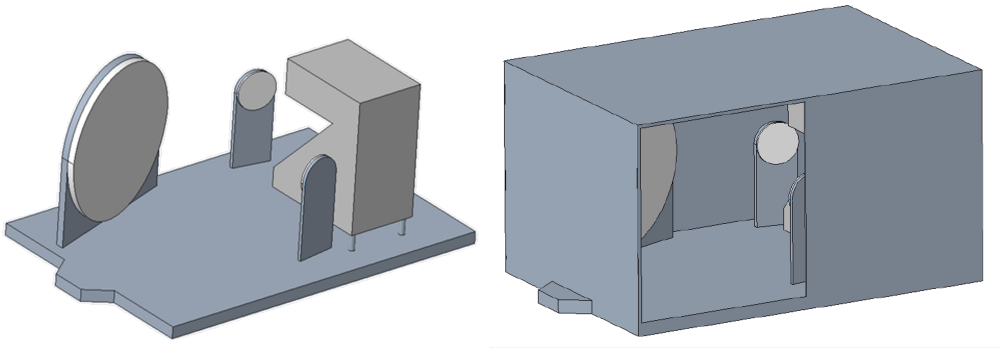

Fig. 3. RIIFS instrument layout without box (left) and with box (right)

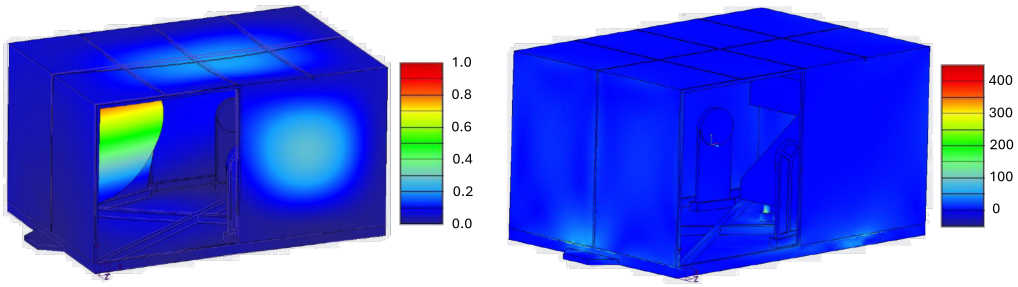

Fig. 4. Left: first modal shape of the RIIFS box; colored scale is normalized displacement. Right: contour plot of the quasi-static loading analyses results; colored scale is Von Mises stress in MPa

Table 1. RIIFS stiffening geometrical properties and simulations results summary

Geometrical parameters	values	Simulation results	
Base plate thickness	2.5 mm	Structure mass	2.01 kg
Base plate ribs height	7 mm	1st mode frequency	151 Hz
Wall thickness	0.5 mm	MOS – X direction	3.1
Wall ribs height	2 mm	MOS – Y direction	10.2
		MOS – Z direction	6

of the mass budget located for the full-size mirror which was 460.37 g. The main dimensions of the flexures were parameterized for each mirror to obtain the desired stiffness in the axial direction while still maintaining radial compliance.

The final designs are presented in Figure 5, alongside their masses.

The mirrors support have been designed exploiting Generative Design (GD), which is a tool that utilizes Artificial Intelligence (AI) algorithms to provide design solutions that ad-

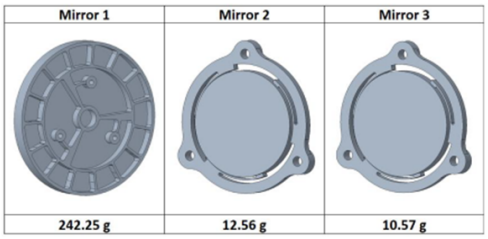

Fig. 5. Final TMA mirrors designs and masses

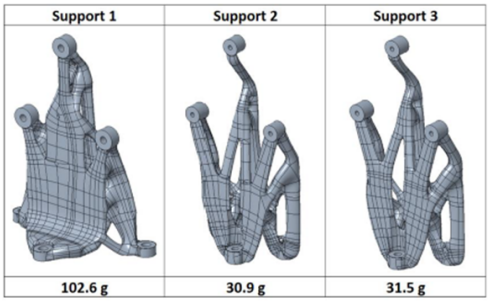

Fig. 6. Supports design obtained by GD

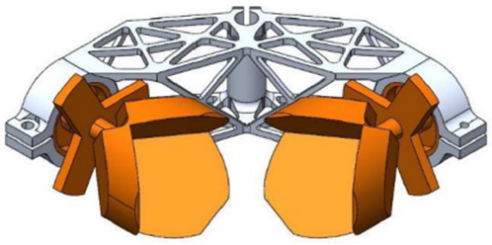

Fig. 7. Cubic mirror holdings final geometry

here to established design criteria such as the loading condition, the size of the working volume and the manufacturing technology, which was set to be AM. For this reason, the material has been changed to AlSi10Mg. Following Figure 6 and Table 2 report the geometries of the obtained solutions and the results of the modal and quasi-static analyses. Eventually, the supports and structures have been assembled and the simulations run again, to assess the behavior of the assemblies. The results are reported in Table 3. The lowest natural frequency is associated with Assembly 1 and is equal to 369 Hz. The MoS of all the assemblies are positive, hence the design is satisfactory Appiani et al. (2023a).

3.3. Cubic mirror holdings

The cubic mirrors holding structure is very important for the interferometer performances because the shape of the vibrational modes of this system determine the sensitivity to mechanical vibrations. Creating a stiffer structure is therefore not only relevant for the launch phases but even more for the operative ones. For these structures, density-based Topology Optimization (TO) has been adopted as designing tool, selecting as material AlSi10Mg to allow the manufacturing of the obtained geometries. After preliminary studies on single-arm configuration, it has been decided to evaluate the redesign of the assembly as a whole, comprising the two arms and the shaft connection, to obtain a lighter solution and the removal of many fasteners. Based on the results obtained by TO, the geometry has been regularized and the final one reported in Figure 7 has been obtained, having a mass of 25.60 g against the about 70 g of the original one.

FE analyses conducted on the obtained model resulted in a first natural frequency of 445 Hz, well above the required limit, and a maximum stress of 123 MPa, obtained by applying an acceleration of 1386 m/s^2 in all axis and axis combination, calculated according to standard ECSS-E-ST-32-10C Rev.2 representing the landing condition and yielding a MoS of 0.63 assuming a FoS of 1.2. The design fulfills the requirements, showing a mass equal to 37% of the original components.

3.4. Optical Bench

The redesign of the Optical Bench (OB) aimed both at exploiting novel design techniques as well as solving a structural interference arising from the adoption of the newly developed double pendulum assembly. For this component an hybrid parametric approach has been adopted, consisting of a first step of model defeaturing and structural modification to accommodate the new double pendulum, followed by a TO process to identify the positions of ribs and reinforcements to be added. Two different configurations have been developed by regularizing the geometries obtained by the TO, one to minimize the overall mass (Configuration A) and one to maximize the dynamic behavior (Configuration B). The optical configuration of each ribbed geometry has been identified by means of a parametric design acting on the orientations and thicknesses of each el-

Table 2. Supports modal and quasi-static analyses results

Property	Support 1	Support 2	Support 3
Mass [g]	36.34	30.9	31.5
MOS	5.95	7.24	7.86
Mode 1 [Hz]	438	856.1	1010.7

Table 3. Simulations results for the assembled structures

	Maximum Von Mises Stress [MPa]			MOS
Assembly #	100 g – X	100 g – Y	100 g – Z	
1	156	238	212	0.2
2	50	64	61	5.3
3	49	63	43	5.5

Modes #	Assembly #		
	1	2	3
M1	369	803	850

ement. The two configurations are reported in the following Figure 8.

Eventually, the performances of the solutions have been assessed by means of FE analyses, whose results are reported in the following Table 4 showing satisfactory results both for modal and quasi-static analyses Saggin et al. (2022). Both obtained solutions allow to solve the mounting problem associated with the new double pendulum group, requiring the removal of a large wall of the actual OB, which was non-trivial since it caused a loss of torsional stiffness of the bench. In specific, Configuration A allows a mass saving of 15% and comparable dynamic behavior, while Configuration B have a similar mass compared to the actual OB but increased performances.

4. Data processing

The second aspect of the development is making the instrument more tolerant to mechanical disturbances. The influence of mechanical disturbances on FTS is well known Saggin et al. (2007b), Saggin et al. (2011), causing the acquisition to occur at non constant steps of the optical path difference and leading to corrupted spectra. Mechanical disturbances affected the quality of some space borne instruments, like Mariner IRIS, Venera 15 FTS, Voyager IRIS, TES-MGS, PFS-MEX Formisano et al. (2005), Persky (1995). The effects can however be mitigated by adopting suitable data acquisition strategies. The approaches pursued in this study are avoiding the direct sampling at "hardware generated constant OPD", by using a high frequency sampling of both the metrology and the science channel and then, through data processing, computing the interferogram sampled at constant OPD steps. More in detail, the first proposed approach involves the direct phase computation of the arccosine function of the metrology channel. Eventually a second approach has been developed based on the previous one but exploiting two reference channels generated from the same laser with a suitable phase shift, leading to a single phase obtained by a combination of the two Appiani et al. (2023b). The performances of the two methods have been compared with the ones of Hilbert's transform-based method, a previously developed technique, which however has some limitations when the frequency of the disturbances approaches specific value, i.e., the nominal frequency of the metrology channel, making this method only applicable in a limited bandwidth. The comparison on the performances of the methods was performed by the calculation of an index, the Normalized Mean Root Square Error (NMRSE), which compares line by line the spectra obtained with the dif-

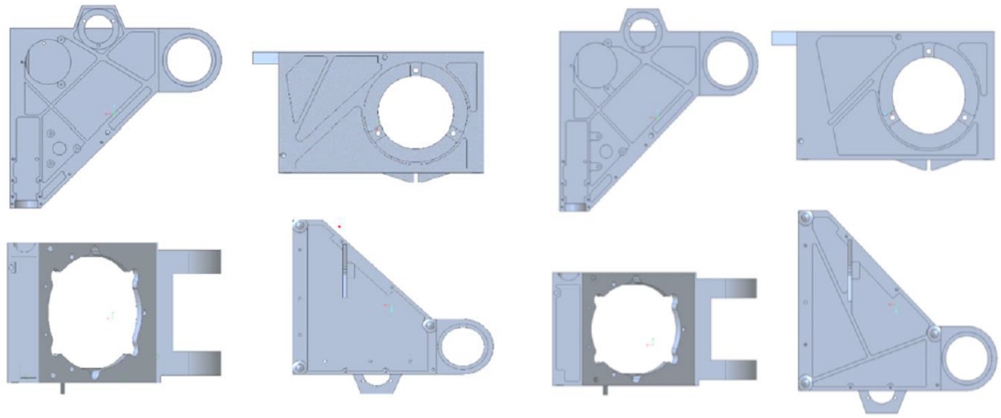

Fig. 8. Optical bench configurations. Left: Configuration A. Right: Configuration B

Table 4. Simulation results and mass for the different OB configurations

OB model	Mode 1 [Hz]	Mode 2 [Hz]	Mass [g]	X [MPa]	Y [MPa]	Z [MPa]	MOS
Actual OB	655	824	158	251	64	212	0.60
Config. A	602	784	135	384	134	205	0.05
Config. B	655	797	149	212	69	243	0.66

ferent approaches. The index is defined as following:

$$NMRSE = 100 \times \frac{\sqrt{\sum_{n=1}^{N}(A_{calc,i} - A_{id,i})^2/n}}{A_{id,max}}$$

where $A_{calc,i}$ and $A_{id,i}$ are the amplitudes of the i-th component (i.e., the i-th single spectral line) of the corrected and ideal spectrum respectively, $A_{id,max}$ is the maximum amplitude in the ideal spectrum and n is the number of spectral lines in the spectra, which has been set equal to 10000. The spectra used for the comparison are obtained starting from interferograms affected both by mono harmonic speed disturbances and Gaussian White Noise (GWN). Figure 9 shows an example of the influence of mono harmonic vibrations on a spectra of a monochromatic source. By looking at the spectrum with disturbances it is possible to observe the onset of some ghost spectral lines.

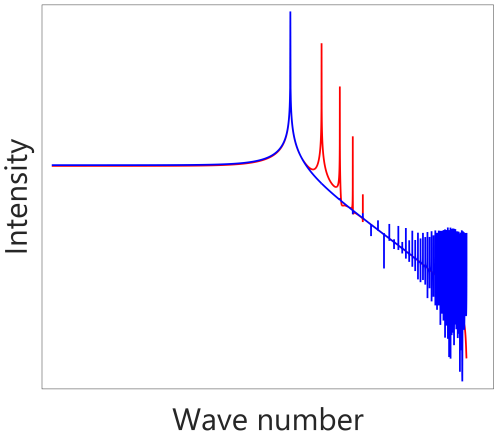

Fig. 9. Comparison of spectra of a monochromatic source. Blue line is the ideal spectrum, red line is the spectrum obtained by an instrument subjected to a mono harmonic speed disturbance during the acquisition

The following graphs in Figure 10 present the NMRSE obtained by simulation for two levels of mono harmonic speed disturbance (20% and 40% of the nominal speed of the mirror) and two levels of SNR (40 dB and 20 dB).

It can be noticed that in general, direct phase determination methods performed better than the Hilbert one when increasing the amplitude of the disturbance, the noise, or both. Moreover, the proposed methods show a regular trend of NMRSE, while Hilbert's method shows significant jumps in correspondence of the carrier frequency and its double, making it unsuitable in case of disturbance frequency above the carrier one. Concerning the direct phase computation methods, the single arc cosine method and the two channels method behave similarly when the noise level is low, even if the amplitude of the disturbance increases, while the NMRSE of the combined phase method shows an improvement at the increase of the noise level.

5. Electronics design and tests

The architecture of the electronic system proposed for this work at bread-board level is shown in Figure 11. The functionality can be divided in two parts, the digital and the analog blocks. This electronic system, that controls the double pendulum motion, is composed of a reference laser, a fringe photodiode and an amplifier that drives a piezoelectric bender actuator. The pendulum velocity depends on the slope of a ramp signal generated by a DAC module. The interferogram can be recorded by two detectors: a single pixel PbSe detector (1 mm pitch), used to test the interferogram acquisition technique or an array of 256 pixel, used to test the imaging capabilities. At the start of the interferogram measurement, during pendulum motion an ADC module samples the signals from the photodetectors in the time domain. All the instrument operations and the communication with a computer are controlled by a micro-controller board. Interferogram data are stored directly on the PC through the USB port. The analog blocks includes the front-end electronics for the PbSe photodetector, together with the conditioning circuit, and the photodetector circuit for the reference laser. Different components or sensors present in the system may need to be stabilized in temperature, such as the PbSe photodetector or the reference laser. The ATC module, Automatic Temperature Control, measures and controls the temperature value in different points of the instrument in order to reduce the signals fluctuations of the sensors to be measured due to the environmental temperature changes. Finally, a power supply module is used to power all the circuits in the system employing many switching mode regulators in accordance with the voltage needed.

For the photodetector array version of the interferometer, the electronic architecture of the system is shown in Figure 12. In this configuration, the front-end used for the single sensor is replaced by a custom board to manage the pixel array. The electronic architecture of the custom board to drive the 256 PbS array detector is shown in Figure 13. All bias and supply voltages are generated on board and a Thermoelectric Cooling (TEC) controller is present to thermalize the sensor. The acquired data are transferred to the PC through a USB port. The piezoelectric motors available are all ceramic bending bi-morph actuators with high bidirectional displacement which are controlled by custom electronics with a ramp signal in order to span the optical path. A 16bit resolution DAC module is employed to control the motor speed according to the scheme. The piezo amplifier module by the PI company has been used to carry out the preliminary tests. The reference laser is used in order to measure the pendulum motion. For preliminary test of the instrument a robust and high quality Coherent® VHK™ Circular Beam Visible Laser Diode has been used, at 4.9 mW and wavelength at 635 nm. To measure the movement of the pendulum, a photodetector is used to receive the interfered signal of the reference laser. The photodetector used for this purpose is a silicon photodiode PDB-C100. The schematic of the photodetector front-end is shown in Figure 13. Due to the noise characteristic of a PbSe photodetector, it is generally suited for AC coupled operation. A DC

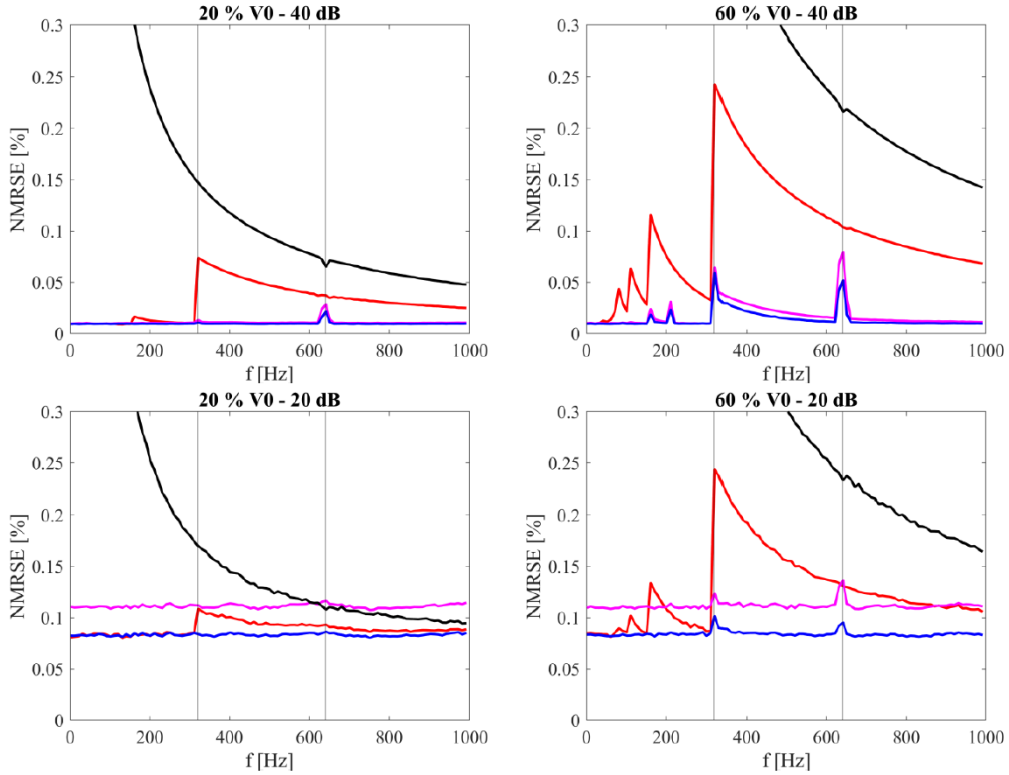

Fig. 10. NMRSE obtained with different correction algorithms. Red: Hilbert transform based correction method; magenta: arccosine correction method; blue: combined phase correction method; black: not corrected

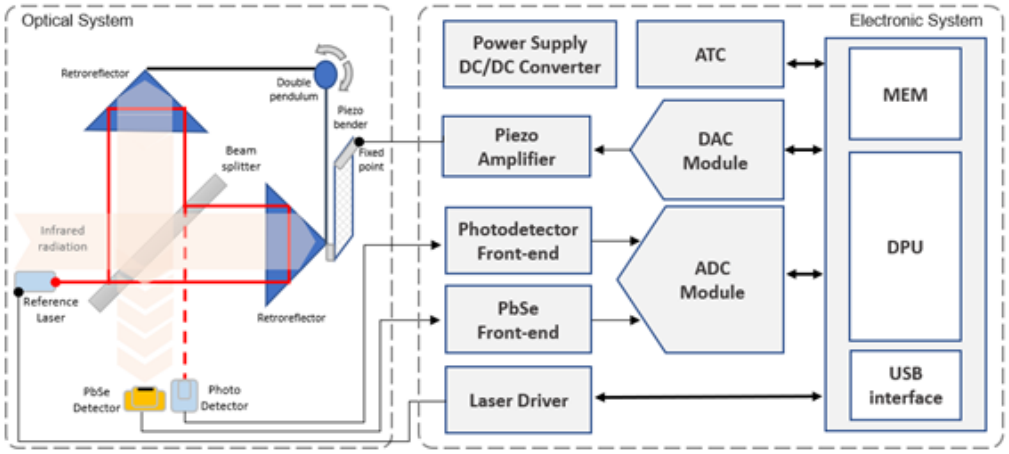

Fig. 11. Electronic System Architecture

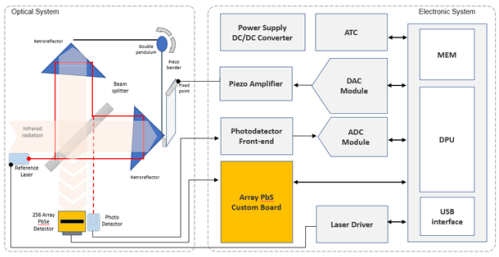

Fig. 12. Architecture of the RIIFS electronics with 256 array PbS detector

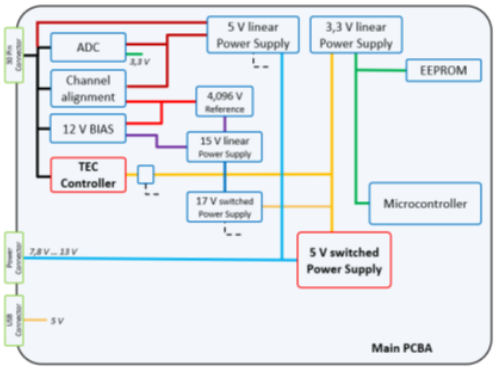

Fig. 13. Architecture of the custom board to drive the 256 PbSe array detector

bias voltage is needed to conditioning the work point of the detector and it should be at a level where the detector SNR is acceptable and maximum. For this reason, IR detectors are normally AC coupled to limit the noise. In order to achieve highest B1-5 photodetector SNR the bias voltage should be between 40 and 50 volt but is very important to consider other voltage noise source to generate an high voltage bias. It is also important to note the high pass filter that AC couples the input of the amplifier blocks any DC signal. In addition, the resistance of the load resistor (RLOAD) should be equal to the dark resistance of the detector to ensure maximum signal can be acquired. A preamplifier is required to help maintain the stability and provide a large gain for the generated voltage signal. Hence, the signal is amplified and provided at the output. In order to eliminate aliasing effects, during digital sampling of the PbSe signal, an 8th order anti-aliasing low-pass filter

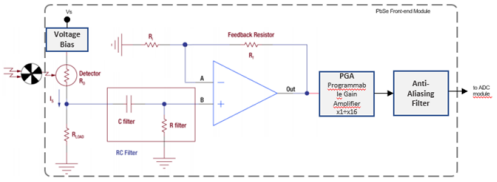

Fig. 14. PbSe detector front-end

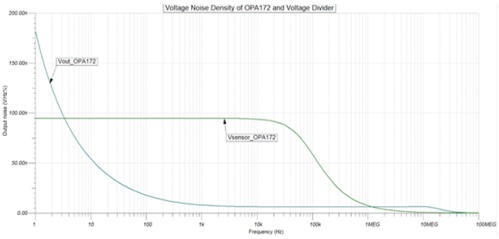

Fig. 15. Simulation of pre-Amplifier noise

is added to the analog chain. For this application the Bessel filter is chosen because it is low noise and acts as a delay line.

The system noise of the sensor front-end is one of the critical aspects of instrument. Aspects on electronic noise have been considered to select the operational amplifier to be used as a preamplifier. Several operational amplifiers have been evaluated to determine the electronic noise level. Amplifiers with comparative features are listed in the Table 5.

For preliminary test the preamplifier the OPA172 commercial op-amp has been selected. In Figure 15 is reported the simulation data of noise density for sensor and OPA172 amplifier. In this configuration the voltage noise is the dominant factor. The actual front-end system noise is 3μV RMS in band of 10kHz. The final system noise becomes 32μV RMS when the detector is connected to the electronic at room temperature. The ADA4610 op-amp is suitable for space applications.

It is important to note that for this project, the bandwidth of interest where noise needs to be minimized is from 100Hz to 2kHz. As we can see in the Figure 15 the level of OPA172 noise density within this bandwidth is lower than the intrinsic noise of the PbSe detector ($90.7\ \text{nV}/\sqrt{Hz}$). This means that the noise introduced by opamp is lower than the intrin-

Table 5. List of the op-amp for PbSe preamplifier

	OPA627	LT1055	**OPA172**	ADA4610
Input Noise Voltage ($\mu V_{P\text{-}P}$) f = 0.1 Hz to 10 Hz	0.6	1.8	2.5	0.45
Input Noise Voltage Density (nV/ $\sqrt{Hz}$) f = 1 kHz	5.2	14	7	7.3
Input Noise Voltage Density (fA/ $\sqrt{Hz}$) f = 1 kHz	1.6	1.8	1.6	3
Input Bias Current (pA)	1	10	8	5
Supply voltage (V+ – V–)	36 (±18)	36 (±18)	36 (±18)	30 (±15)
Quiescent current per amplifier (mA)	7	2.8	1.6	1.6
Specified temperature (°C)	–40 to 125	0 to 70	–40 to 125	–40 to 125
GBWP (MHz)	16	4.5	10	16.3

sic noise of the photodetector at room temperature and therefore can be neglected. In the single PbSe photodetector configuration the analog/digital converter (ADC) choice is another critical aspect. The signals from the PbSe photodetector and the photodiode, after being amplified and filtered, are acquired by an ADC. For the final version of the project, the ADS1278 delta-sigma converter will be used. This converter allows simultaneous sampling of eight channels with data rates up to 144k samples per second in high-speed mode and 52k samples per second in high-resolution mode. ADS1278 combine high-precision industrial measurement with excellent dc and ac specifications. The high-order, chopper-stabilized modulator achieves very low drift with low in-band noise. The onboard decimation filter suppresses modulator and signal out-of-band noise. These ADC provide a usable signal bandwidth up to 90% of the Nyquist rate with less than 0.005dB of ripple. Optical systems, light sources and conditioning electronics are integrated in a test bench with laboratory equipment for preliminary test and system performances. Two photodetectors are tested: single PbSe detector and 256 PbS array. Figure 16 shows the test bench for testing the developed interferometer. Figure 17 shows the two versions of the interferometer according to the used photodetector.

For single PbSe detector the conditioning electronic is placed near the sensor as shown in Figure 18. The signals out from photodetector are sent to a data acquisition system NI USB-6218 that also generates the analog signal for driving piezoelectric motors.

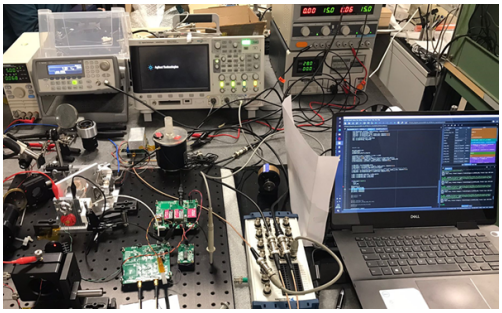

Fig. 16. Test bench for RIIFS project

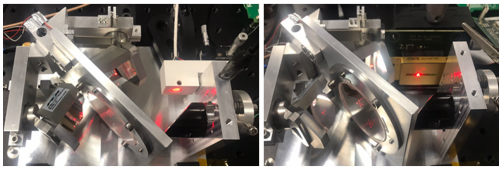

Fig. 17. Interferometer with single PbSe photodetector (left) and 256 PbS array photodetector (right)

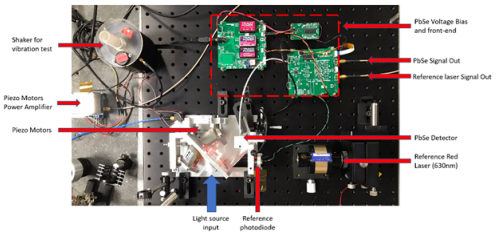

Fig. 18. Sensors and actuators connection

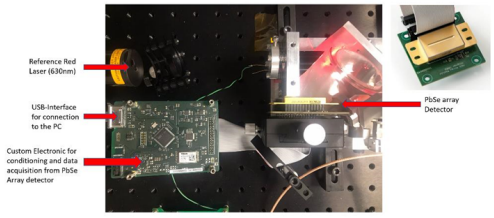

Fig. 19. Placement and connection of 256 PbS array detector

For PbS array detector a custom electronic board has been developed, as shown in Figure 19. The signals out from array sensor are sampled and directly sent to a PC trough USB port. Also in this configuration, the system NI USB-6218 generates the analog signal to drive piezoelectric motors.

To assess vibration immunity, a shaker connected to a function generator (Agilent 33210A) has been placed on the optical table, as shown in Figure 20, and the data acquisition system (NI USB-6218) generates all the signals needed to drive the interferometer. A piezoelectric accelerometer has been placed for feedback of the vibration level generated by the shaker. Acceleration has been acquired through Apollo Box Data Acquisition System with 24-bit ADC and USB Interface. In Figure 21 the spectrum of an Helium-Neon laser at 632 nm is shown. The width of the spectral line is determined by the maximum optical path difference, providing a resolution of 0.1268 nm at 635 nm or 3.155 cm^{-1}. In Figure 22 we show the same spectral line when some mechanical disturbances are applied. On the left the double pendulum velocity and the spectrum are shown when the shaker is off. On the right panels the same, but with the shaker on. The intensity of disturbances is about 28 times higher with respect the previous case. It can be seen that no spectral artifact due to the higher mechanical noise are present in the spectrum.

6. Conclusions

In this paper we described the activities done during the instrument study funded by ASI. This work has lead to a laboratory breadboard on which the new interferogram sampling technique has been implemented, assessing the immunity to mechanical vibration and the capability to operate during thermal transients. Optical-radiometric and thermomechanical analysis have been run to assess the applicability on different solar system bodies and the impact on instrument performances. The present status of the activities is the following:

- RIIFS is a Fourier transform spectrometer with the interferometer module based on the MIMA design (TRL=5). During the study we have designed a telescope to reduce the field of view and providing imaging capabilities.
- A review of possible scientific applications has been done. These include spectroscopic investigation (resolving power 40-1000) of both planetary surfaces and atmospheres in the 2 – 25 micron wavelength range. This spectral interval can be covered by using different detectors (PbS, PbSe, HgCdTe, microbolometer or pyroelectric).
- A review of both scientific (radiometry, angular and spectral resolution) and technical (mass, size, power, available technology) requirements has been done.
- The instrument can work either at room or lower temperatures. In the former case, either PbS, PbSe or pyroelectric single pixel detectors (no imaging) can be used. If imaging capabilities are required, a microbolometer matrix can be used, working at room temperature. If higher sensitivity is needed, the instrument must be cooled and the detector is a HgCdTe matrix. In this case, the overall mass could exceed the 5 Kg current baseline.
- As far as the overall TRL is concerned, we must distinguish two options:

1. Option #1. The instrument is a single pixel spectrometer working at room temperature. Based on previous experience (PFS/MeX and MIMA/Exomars) this instrument configuration, compared to Option #2, has

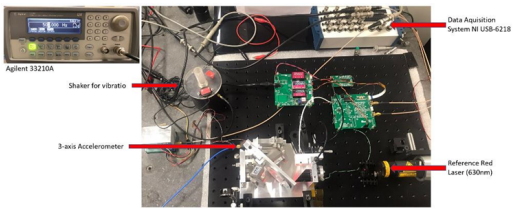

Fig. 20. Vibration immunity set-up

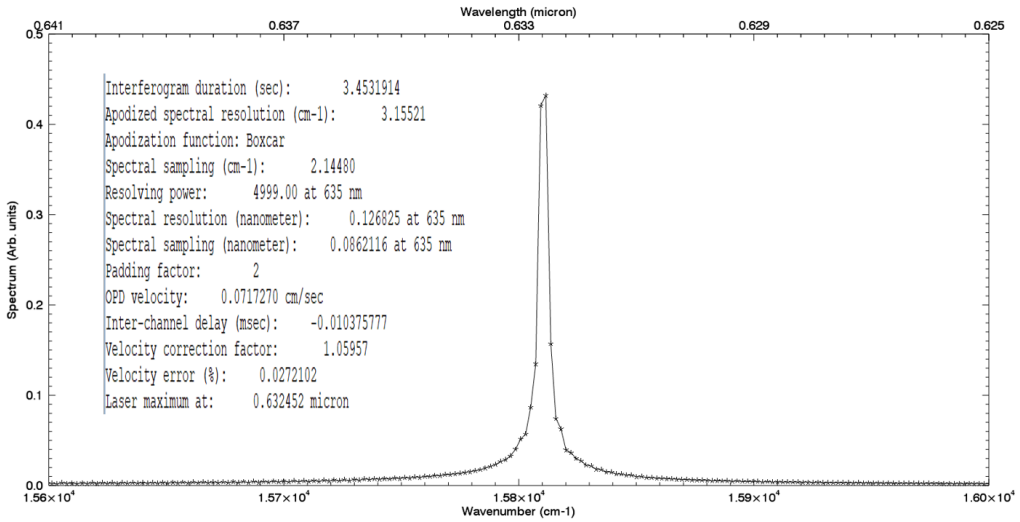

Fig. 21. He-Ne laser line as resolved by the RIIFS spectrometer. Instrumental parameters are indicated in the legend.

been investigated and tested in more detail and presents less areas of concern. Since we have added a telescope, this will require some additional design effort. Even if the TMA design is well established, its actual manufacturing design and coupling to the interferometer unit should be better investigated (e.g. position of the field stop, calibration unit, stray light). As far as electronics is concerned, we do not see particular problems, since the volume is enough to allocate 3 boards with space qualified components. The detector can work either at room temperature or cooled e.g. by a small radiator (in the case of PbS and PbSe). Both telescope and interferometer can stay at room temperature.

2. Option #2. Instrument with a matrix detector. In this case, unless the detector is an uncooled mircobolometer, the telescope+interferometer must be passively cooled at 130-220K, depending on the requested scientific performances (mainly SNR, spectral and spatial resolution). In this case the detector is a HgCdTe matrix and actively cooled at 80K. While the thermo-mechanical design can guarantee the instrument performances at 130-180K (the MIMA interferometer optical alignment has already been verified down to 130K), an instrument breadboard must be developed to check the functionality.
3. For both options, the flight unit design will require some additional work of optimization of the integrated system, being the

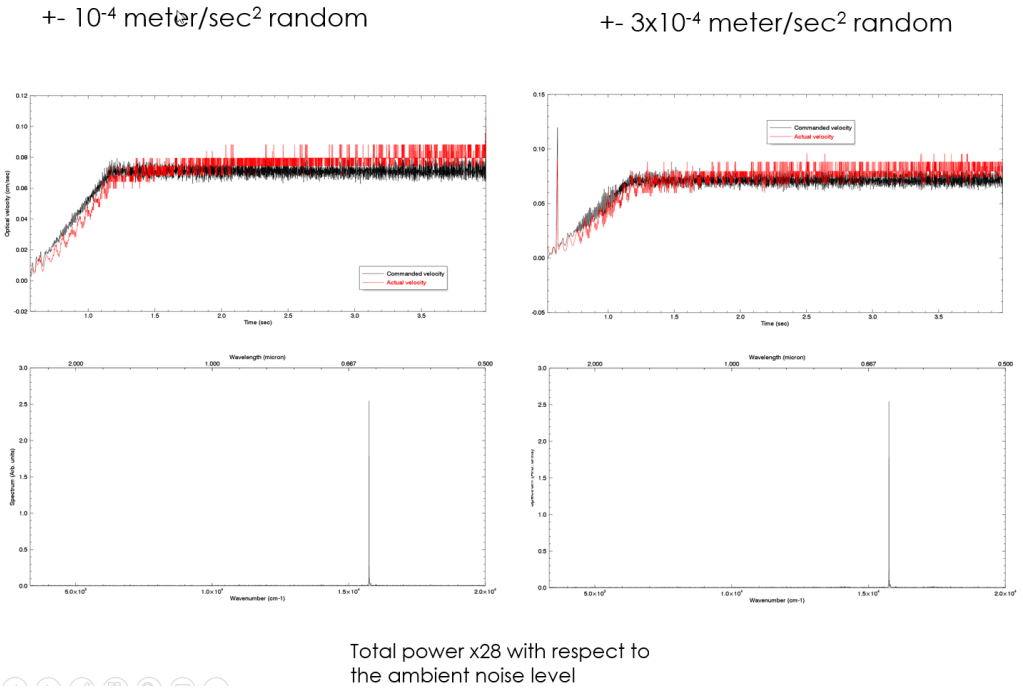

Fig. 22. On the left the double pendulum velocity and the He-Ne laser line spectrum are shown. The intensity of the mechanical noise (ambient level) is indicated. On the right the same but with the shaker on.

maturity level of the interferometer design (MIMA inherited) quite different from that of the new developed telescope.

Acknowledgements. We are gratefully to the Italian Space Agency for funding the RIIFS project through grant 2018-16-HH.0

References

Appiani, A., Saggin, B., Amui, I., et al. 2023a, in 2023 IEEE 10th International Workshop on Metrology for AeroSpace (MetroAeroSpace), 89–93

Appiani, A., Scaccabarozzi, D., & Saggin, B. 2023b, in 2023 IEEE 10th International Workshop on Metrology for AeroSpace (MetroAeroSpace), 136–140

Bellucci, G., Saggin, B., Fonti, S., et al. 2007, in Society of Photo-Optical Instrumentation Engineers (SPIE) Conference Series, Vol. 6744, Sensors, Systems, and Next-Generation Satellites XI, ed. R. Meynart, S. P. Neeck, H. Shimoda, & S. Habib, 67441Q

Christensen, P. R., Bandfield, J. L., Hamilton, V. E., et al. 2001, J. Geophys. Res., 106, 23823

Fonti, S., Marzo, G. A., Politi, R., Bellucci, G., & Saggin, B. 2007, in Society of Photo-Optical Instrumentation Engineers (SPIE) Conference Series, Vol. 6744, Sensors, Systems, and Next-Generation Satellites XI, ed. R. Meynart, S. P. Neeck, H. Shimoda, & S. Habib, 67441R

Formisano, V., Angrilli, F., Arnold, G., et al. 2005, Planet. Space Sci., 53, 963

Hamilton, V. E. & Christensen, P. R. 2000, J. Geophys. Res., 105, 9717

Hanel, R. A., Conrath, B. J., Jennings, D. E., & Samuelson, R. E. 2003, Exploration of the Solar System by Infrared Remote Sensing: Second Edition (Cambridge University Press)

Henini, M. & Razeghi, M. 2002, Handbook of Infrared Detection Technologies (Elsevier Science Publishers)

Persky, M. J. 1995, Review of Scientific Instruments, 66, 4763

Ramsey, M. S. & Christensen, P. R. 1998, J. Geophys. Res., 103, 577

Rogers, A. D., Bandfield, J. L., & Christensen, P. R. 2007, Journal of Geophysical Research (Planets), 112, E02004

Saggin, B., Alberti, E., Comolli, L., et al. 2007a, in Society of Photo-Optical Instrumentation Engineers (SPIE) Conference Series, Vol. 6744, Sensors, Systems, and Next-Generation Satellites XI, ed. R. Meynart, S. P. Neeck, H. Shimoda, & S. Habib, 67441S

Saggin, B., Comolli, L., & Formisano, V. 2007b, Appl. Opt., 46, 5248

Saggin, B., Scaccabarozzi, D., Appiani, A., et al. 2022, in 2022 IEEE 9th International Workshop on Metrology for AeroSpace (MetroAeroSpace), 107–112

Saggin, B., Scaccabarozzi, D., & Tarabini, M. 2011, Appl. Opt., 50, 1717